Full length article

Fabrication of hASCs-laden structures using extrusion-based cell printing supplemented with an electric field

MyungGu Yeo [1], JongHan Ha [1], HyeongJin Lee, GeunHyung Kim *

Department of Biomechatronic Engineering, College of Biotechnology and Bioengineering, Sungkyunkwan University, Suwon, South Korea

ARTICLE INFO

ABSTRACT

In this study, we proposed a hybrid cell-printing technique that combines a conventional extrusion-based cell-printing process with an electrohydrodynamic jet. The electric field stabilized the extruded struts of cell-embedding-hydrogel and reduced the damage to dispensed cells caused by the high wall shear stress in the dispensing nozzle. The new cell-printing process was optimized in terms of various processing parameters, applied electric field strength, nozzle movement speed, and distance between the nozzle tip and working stage. Using the optimal cell-embedding hydrogel composition (1×10^6 cells mL^{-1} in 4 wt% alginate) and cell-printing process parameters (applied voltage, 1 kV; nozzle movement speed, 12 mm s^{-1}; distance, 0.7 mm; current, 10.67 ± 1.1 nA), we achieved rapid and stable fabrication of a cell-laden structure without loss of cell viability or proliferation, the values of which were similar to those of the process without an electric field. Furthermore, by applying the same pneumatic pressure to fabricate cell-laden structures, considerably higher volume flow rate and cell viability at the same volume flow rate were achieved by the modified process compared with conventional extrusion-based cell-printing processes. To assess the feasibility of the method, the hydrogel containing human adipose stem cells (hASCs) and alginate (4 wt%) was fabricated into a cell-laden porous structure in a layer-by-layer manner. The cell-laden structure exhibited reasonable initial hASC viability (87%), which was similar to that prior to processing of the cell-embedding-hydrogel.

Statement of Significance

The extrusion-based cell-printing process has shortcomings, such as unstable flow and potential loss of cell viability. The unsteady flow can occur due to the high cell concentration, viscosity, and surface tension of bioinks. Also, cell viability post extrusion can be significantly reduced by damage of the cells due to the high wall shear stress in the extrusion nozzle. To overcome these limitations, we suggested an innovative cell-printing process that combines a conventional extrusion-based cellprinting process with an electric field. The electric field in the cell-printing process stabilized the extruded struts of bioink and dramatically reduced the damage to dispensed cells caused by the high wall shear stress in the dispensing nozzle.

1. Introduction

Tissue engineering has developed rapidly during the last decade. The technique facilitates regeneration of a variety of damaged tissues and organs. To successfully regenerate various tissues, polymeric scaffolds have been widely used. These scaffolds should generate nontoxic byproducts during degradation and have good biocompatibility and appropriate mechanical properties [1]. In addition, highly porous structures provide paths for the transport of nutrients and metabolic waste and induce vascularization *in vivo* [2]. Using scaffold-based tissue engineering, damaged tissues and organs, including bladder [3], myocardium [4], skin [5], cartilage [6,7], and bone [8], have been treated effectively. However, despite the advantages of scaffold-based tissue engineering, several issues remain, including low cell-seeding efficiency, inhomogeneous cell growth after prolonged culture, and difficulty embedding cells in the desired region of the scaffold [9,10].

* Corresponding author at: Department of Biomechatronic Engineering, College of Biotechnology and Bioengineering, Sungkyunkwan University, Suwon 440-746, South Korea.

E-mail address: gkimbme@skku.edu (G. Kim).

[1] These authors contributed equally to this study.

One potential solution to these problems is a cell-printing process, which offers the advantages of flexible cell retention, homogeneous distribution of cells at the required locations, and efficient delivery of growth factors [10–14]. Several cell-printing techniques are available, including extrusion [15], laser [16], microvalve [17], inkjet [18], and heterogeneous cell-laden processes [19]. For example, Koch et al. successfully fabricated a 20-layer fibroblast- and keratinocyte-laden collagen structure mimicking natural skin using a laser-based bioprinting process [20]. Also, Xu et al. demonstrated a new technique to manipulate cell-encapsulating microscale hydrogels using acoustic waves, which can be utilized in regenerative medicine and cell/drug delivery [21]. In the study by Fuh [22], L929 rat fibroblasts were successfully delivered through a nozzle (36 μm in diameter) using an inkjet technique. Kolesky et al. [19] fabricated a heterogeneous 10T1/2 fibroblast-laden structure with vasculature using a cell carrier, gelatin methacrylate, and a three-dimensional (3D) co-printing method [19]. The results suggested a new approach to the design of 3D cell-laden structures with a micro-engineered environment, which could be useful in drug screening, angiogenesis, and stem cell studies [19].

Of these cell-printing techniques, the extrusion method is considered the simplest process for fabricating 3D scaffolds in which cells can be encapsulated stably. Recently, our research group has proposed several extrusion methods supplemented with aerosol cross-linking [23], a low-temperature processing working stage [24], and a core-shell nozzle [25], to obtain precisely designed macroscale cell-laden structures with micropores and reasonable cell viability.

However, the drawbacks of the extrusion-based cell printing method are unstable flow and potential loss of cell viability. Unsteady flow from a pressurized microscale nozzle can occur due to the high cell concentration in the cell-embedding-hydrogel and its viscosity and surface tension (i.e., Rayleigh–Plateau instability) [26–28]. Also, cell viability can be reduced by damage of the cells [20], the plasma membrane [29], and protein structure [30], due to the wall shear stress in the extrusion nozzle [31] and the prolonged period required to fabricate a highly porous complex structure [32].

Here, to overcome these limitations, we combined extrusion-based cell printing with an electrohydrodynamic jet (EJ) process. The EJ method, originally used in commercial jet printing [33], has been applied to produce liquid alginate beads containing cells [34,35]. L. Gasperini et al. fabricated hollow cylindrical structure containing 3T3 mouse fibroblast cells using an EJ method [34]. However, the proposed EJ technique has several limitations for fabricating precisely designed cell-laden pore structures with high cell viability to replace complex 3D anatomic defects, because the process requires a high electric field strength (12–20 kV) and showed little capability with regard to 3D shape fabrication [34]. Also, cell-electrospinning has been used to obtain a fibrous cell-laden structure [36]. However, the system to obtain the fibrous structure should be required in high electric field strength over 7 kV. Furthermore, the electrospun cell-laden hydrogel fibers can be extremely difficult to fabricate three-dimensionally designed porous structure because the electrospun fibers can be easily merged in each other and the fibers were deposited with the random two-dimensional structure.

In this work, to obviate the need for high electric field strength and overcome the low shapeability, we combined the EJ technique and an extrusion-based cell-printing method. The cell-laden solution was extruded using pressurized air; to reduce the shear stress in the nozzle wall and obtain stable flow of the cell-laden hydrogel, we used an electrostatic force directed to a grounded working stage, similar to the EJ process. The electric field strength applied during the process was 1–3 kV. To prevent high current flow between the nozzle tip and grounded stage, we attached a glass substrate to the working stage. The optimum electric field strength for fabrication of homogeneous cell-laden struts that resulted in high initial cell viability was first determined. After fabrication, cells were cultured in the porous structure for various periods, and the effect of the electric field on their activities was investigated. Based on the work, we can confirm that the pressure-assisted cell dispensing supplemented with an electric field can enable to fabricate much more stable cell-laden struts due to the electrostatic forces between the nozzle and grounded working plate and also provide significantly higher cell viability of the printed struts due to the lowered wall shear stress within the microsize-nozzle compared to the normal pressure-assisted cell dispending method.

2. Experimental section

2.1. Preparation of cell-laden hydrogel

Alginate hydrogels were prepared by the following method, described in our previous work [37]. A mixture of alginate (FMC BioPolymer, Drammen, Norway) and phosphate-buffered saline (PBS) was prepared to obtain a 4 wt% alginate solution. To increase the viscosity of the solution, 0.5 wt% $CaCl_2$ (Sigma–Aldrich, St. Louis, MO, USA) was added at an alginate:$CaCl_2$ ratio of 7:3. Osteoblast-like cells (MG63, CRL-1427; ATCC, Manassas, VA, USA) and human adipose stem cells (hASCs, Anterogen Corporation, South Korea) were added to the solution to a density of 1×10^6 mL^{-1} using a three-way stopcock.

### 2.2. Single-line test of cell-laden hydrogel

To perform a single-line test of cell-laden struts under various electric field conditions, we used a computer-controlled three-axis robot system (DTR2-2210T, Dongbu Robot, Bucheon, South Korea) equipped with a dispensing system (Fig. 1(a, b)). A glass substrate (thickness: 1 mm; microscope glass; Marienfeld, Germany) was used to block the current flow from the nozzle tip (nozzle diameter: 150 μm) to the working stage. A power supply (HVDC, SHV300RD-50K; ConverTech, South Korea) was used to apply the electric field. Because application of high pneumatic pressure to the cell-embedding-hydrogel within the nozzle may reduce cell viability, we applied a moderate pneumatic pressure, 70 ± 10 kPa. The nozzle movement speeds were 6 and 12 mm s^{-1}. The cell-laden alginate solution was loaded into a syringe barrel. An aerosol process using a $CaCl_2$ solution (aerosol flow rate of $CaCl_2$ (5% (w/v) in TBS (Tris-buffered saline), 1.45 ± 0.2 mL min^{-1}) was used to tentatively crosslink the surface of the extruded struts [38] for stable cylindrical strut fabrication (Fig. 1(c)). After fabrication of a single layer, the cell-laden struts were further cross-linked with $CaCl_2$ solution (2% (w/v)) for 2 min (Fig. 1(d)) and rinsed in pure TBS to remove residual calcium ions (Fig. 1(e)).

2.3. Characterization of dispensed cell-laden struts

The dispensed struts were visualized by optical microscopy (BX FM-32; Olympus, Tokyo, Japan) and scanning electron microscopy (SEM, SNE-3000M; SEC Inc., Suwon, South Korea).

2.4. Culture of cell-laden alginate structures

The four-layered cell-laden structures (16 mm × 16 mm × 1.8 mm) were cultured and maintained in minimal essential medium (MEM; Life Science, St. Petersburg, FL, USA) containing ascorbic acid (50 μg/mL), 10-mM β-glycerophosphate, 10% fetal bovine
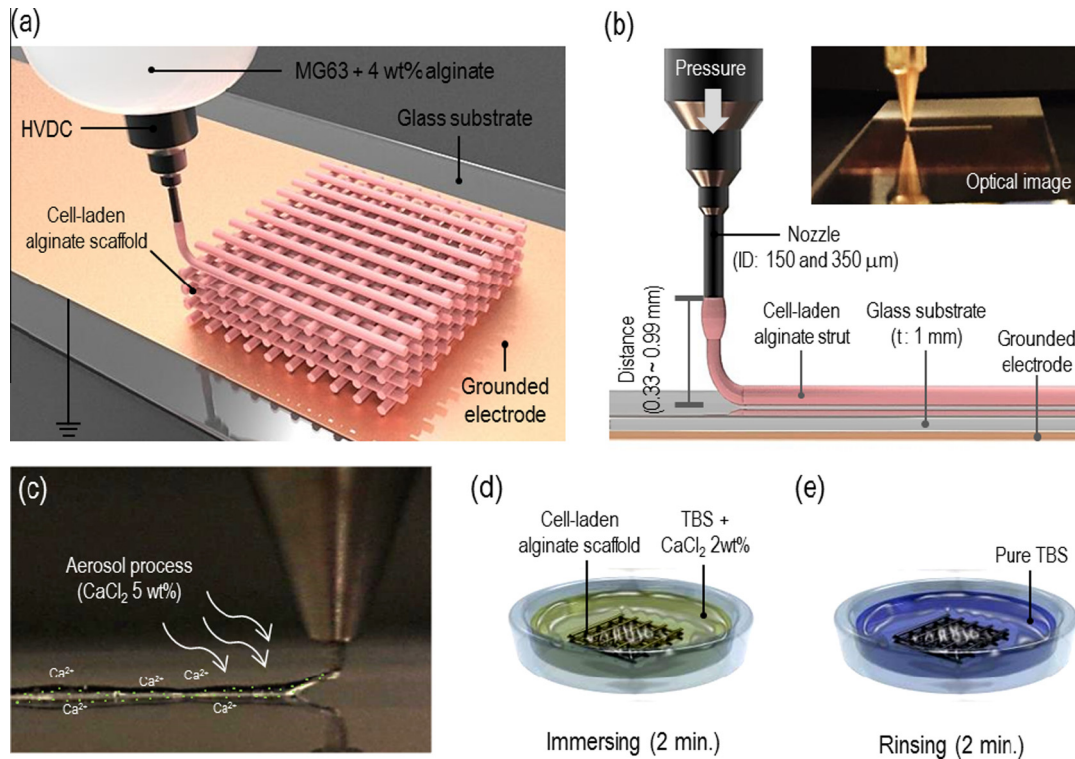
Fig. 1. (a, b) Schematic diagram of the electric-field-supplemented cell-printing process, (c) spraying of 5 wt% CaCl$_2$ aerosol onto a cell-laden strut, (d) second cross-linking in TBS (Tris-buffered saline) with 2 wt% CaCl$_2$ for 2 min post fabrication of cell-laden structures, and (e) final rinsing of the fabricated structure in TBS to remove residual calcium ions.

serum (Gemini Bio-Products, Sacramento, CA, USA) and 1% antibody (Antimycotic; Cellgro, Manassas, VA, USA). The structure was incubated in a 5% CO$_2$ atmosphere at 37 °C, and the medium was changed every second day.

2.5. Live/dead assay of cells post extrusion

To obtain florescence images of live/dead cells, the cell-laden structures were exposed to 0.15-mM calcein AM and 2-mM ethidium homodimer-1 for 45 min in an incubator (37 °C). Stained samples were visualized by fluorescence microscopy. Stained images in which green indicated live cells and red indicated dead cells were captured. The ratio of the number of live cells to the total number of cells (live and dead cells) was calculated using ImageJ software (National Institutes of Health, Bethesda, MD, USA). The value was normalized to the initial cell viability (the value before cell-alginate extrusion) and the initial cell viability was determined by Trypan blue assay (Mediatech, Herndon, VA, USA).

2.6. Cell proliferation and ALP staining

Cell proliferation was determined by 3-(4,5-dimethylthiazol-2-yl)-2,5-diphenyltetrazolium bromide (MTT) assay (Cell Proliferation Kit I; Boehringer Mannheim, Mannheim, Germany). The MTT assay is based on cleavage of the yellow MTT by mitochondrial dehydrogenases in viable cells to generate purple formazan crystals. Cell-laden structures were incubated with 0.5 mg mL^{-1} MTT for 4 h at 37 °C. The absorbance at 570 nm was then measured using a microplate reader (EL800; Bio-Tek Instruments, Winooski, VT, USA). Five samples were used for each incubation period, and each test was performed in triplicate.

After 10 days of cell-culture, for alkaline phosphatase (ALP) staining, cells were washed with PBS twice and equilibrated with

AP buffer (100 mM Tris-Cl, pH 9.5, 100 mM NaCl, and 10 mM MgCl$_2$); NBT and BCIP staining solutions were then applied for 30 min. The reaction was stopped by addition of PBS containing 20 mM EDTA. The osteogenic medium was refreshed every 3 days.

2.7. Statistical analyses

Data are means ± standard deviation. Statistical analyses were performed using the SPSS software (ver. 20.0; SPSS, Inc., Chicago, IL, USA), and included single-factor analyses of variance. In this study, $p < 0.05$ indicated statistical significance. 'NS' indicates no significant difference.

3. Results and discussion

3.1. The effect of electrostatic stress on cell-laden-hydrogel flow and cell viability

To evaluate the effect of the supplemental electric field in the pressure-assisted cell-printing process (PA-CP) on flow stability, we compared a general PA-CP with a modified PA-CP supplemented with electric fields of various strengths. The modified PA-CP supplemented with an electric field is hereafter termed PA-CP-E. In both processes, the pressure applied was 70 ± 10 kPa, and the weight fraction of alginate was 4 wt%.

Fig. 2(a) shows optical images of the nozzle tip during the extrusion process in the PA-CP process and PA-CP-E process using 1, 2, or 3 kV. Cell-embedding-hydrogel flow in the PA-CP process tended to clog the nozzle tip due to the high viscosity of the cell-embedding-hydrogel and its non-homogenous viscosity distribution in the radial direction [26,27]. This may lead to loss of cells during the process and/or delay the fabrication of the 3D cell-laden structure. However, as shown in the images of structures
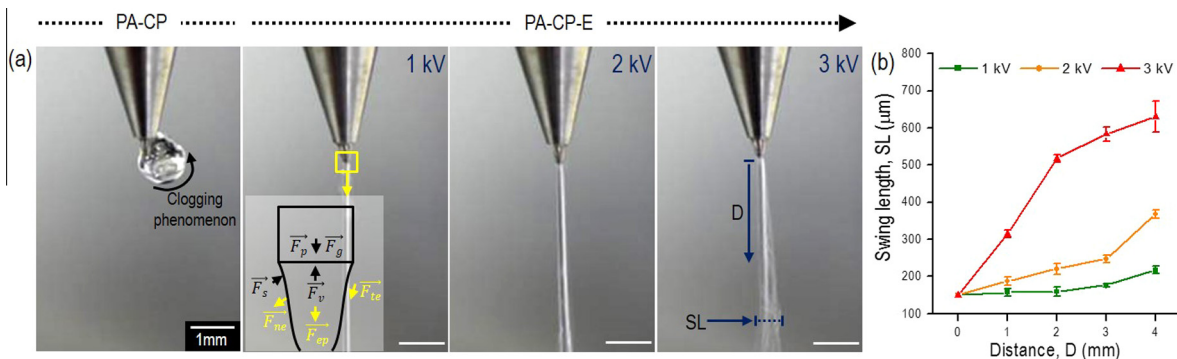
Fig. 2. (a) Optical images of cell-embedding-hydrogel extrusion at the nozzle tip under various electric voltages (PA-CP: pressure-assisted cell-printing process and PA-CP-E: pressure-assisted cell-printing process supplemented with an electric field [1, 2, or 3 kV]). In the 1 kV PA-CP-E image, $\vec{F_p}$, $\vec{F_v}$, $\vec{F_g}$, $\vec{F_s}$, $\vec{F_{ne}}$, $\vec{F_{ep}}$, and $\vec{F_{te}}$ represent forces induced by pressure and viscosity, gravity, surface tension, normal electric stress, electric polarization stress, and tangential electric stress, respectively. (b) Comparison of the swing length (SL), defined in the 3 kV PA-CP-E image, for various distances (D) from the nozzle tip to the working stage.
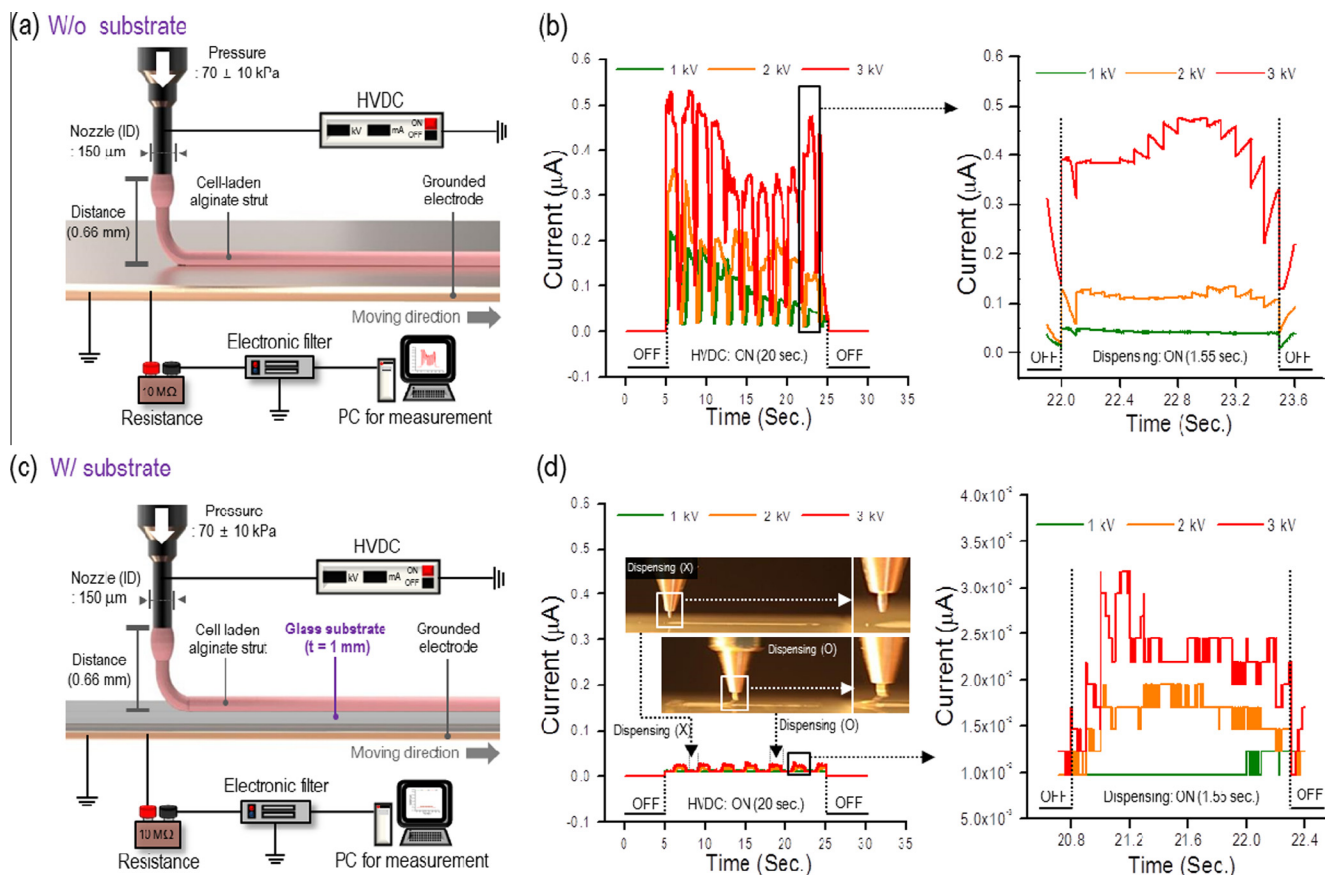
Fig. 3. Schematic diagram of the electric-field-supplemented cell-printing process (a) without a glass substrate to prevent high current flow and (b) the measured current according to the applied electric field strength. (c) Schematic diagram of the printing setup with the glass substrate and (d) the measured current for a given applied electric field strength.

fabricated using the PA-CP-E process, cell-embedding-hydrogel at the nozzle tip was stably extruded (*i.e.*, no clogging occurred) to the working substrate due to the three additional electrostatic forces—normal electric stress ($\vec{F_{ne}}$), electric polarization stress ($\vec{F_{ep}}$), and tangential electric stress ($\vec{F_{te}}$) [40–42]. The normal electric force works in the vertical direction to the surface of the extruded solution, inducing it to swing from side to side, resulting in destabilization of the cone-jet. The tangential and electric polarization forces support the straightness of the charged jet by

moving the cell-embedding-hydrogel to the apex of the meniscus. If the electric tangential force is sufficiently high, a stable cone-jet can be obtained [42]. To evaluate the effect of the normal electric force on jet stability, we measured the swing length (SL) for the distance from the nozzle tip and applied voltages (Fig. 2(b)). The SL of the extruded cell-embedding-hydrogel increased with increasing electric field strength. Although in the PA-CP-E method the electric field eliminated clogging of the nozzle tip, it can also result in unstable flow, such as SL. Thus, the range of the applied electric field must be optimized.
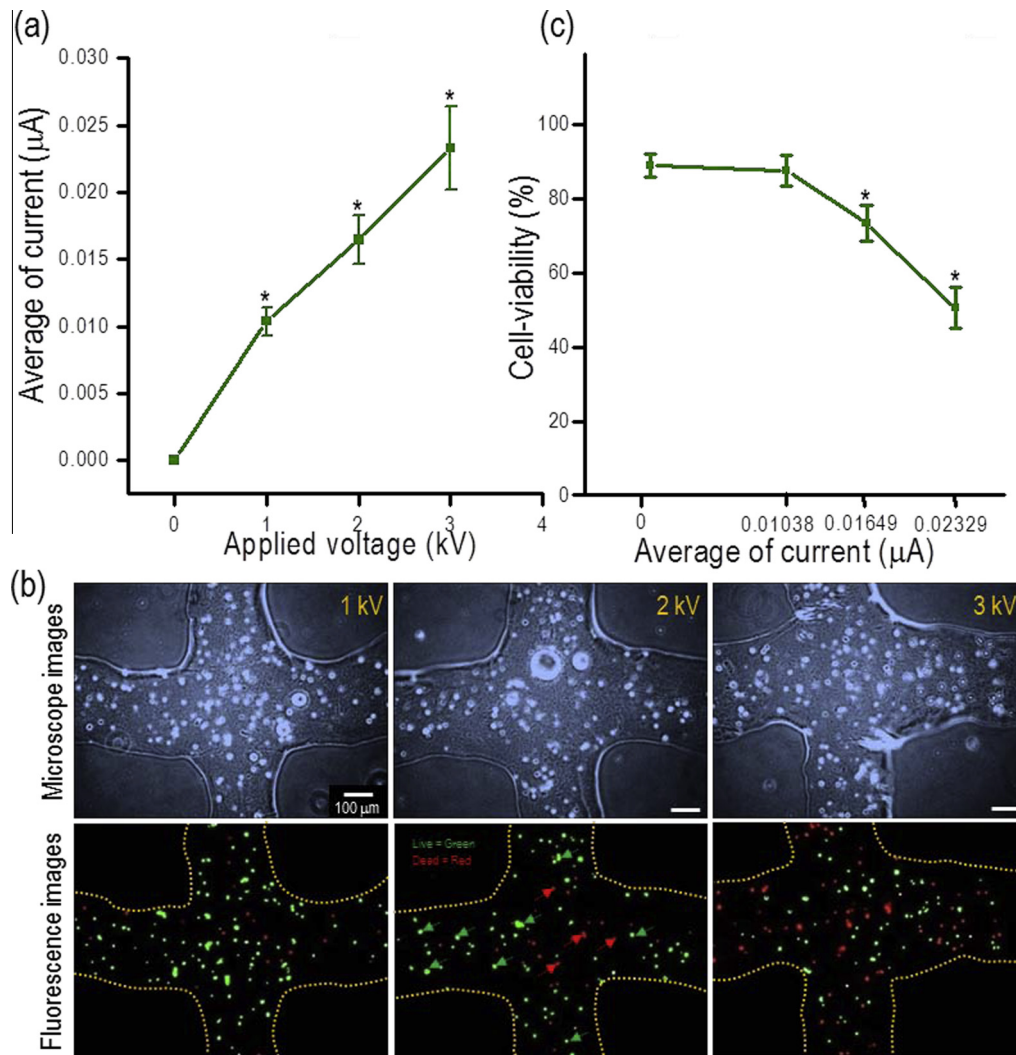
Fig. 4. (a) Relationship between applied voltage and measured current for the printing process with a glass substrate. (b) Micrographs and live (green)/dead (red)-stained images of cell-laden structures fabricated using electric field strengths of 1, 2, or 3 kV. (c) Plot of cell viability (as determined by live/dead staining) versus measured current ($n = 5$). Asterisks (∗) indicate $P < 0.05$. (For interpretation of the references to colour in this figure legend, the reader is referred to the web version of this article.)

Another obstacle to use of an electric field is generation of an electric current during the cell-printing process. However, according to a previous report [43], very low current (nanoampere level) during an electrostatic process does not significantly affect cell viability. In addition, in our previous work, the viability of osteoblast-like-cells (MG63), electrospun using a current of 0.6 μA, was >90%, which was similar to that before the electrospinning process [44].

Fig. 3(a) shows a schematic diagram of the electric current measurement set-up for the grounded electrode during the cell-printing process. The current increased dramatically with increasing electric field strength (Fig. 3(b)), and the current fluctuated with all electric field strengths tested. This was due to the non-homogenous distribution of cells in the hydrogel. Also, the measured currents were in the range of 0.05–0.6 μA; this would not affect some cell types, but may cause damage in others. Therefore, we reduced the electric current by attaching a glass substrate (thickness (t) 1 mm) to the grounded electrode (Fig. 3(c)). As expected, the electric current (10–35 nA) was several-fold lower than that in the absence of the glass substrate (Fig. 3(d)). Thus, our cell-printing process is safer than the EJ cell-printing process.

To assess the effect of the glass substrate on the electric current, we measured the relationship between the applied voltage and the measured current in the cell-embedding-hydrogel (Fig. 4(a)); the relationship was found to be proportionally linear. The effect of the current on cell viability was next determined at 4 h after printing. Fig. 4(b) shows microscopic and fluorescence images (live cells: green; dead cells: red) of a cell-laden structure. The number of red spots increased with increasing applied voltage (current). Interestingly, the cell viability (87.6 ± 4.1%) of cell-embedding-hydrogel subjected to the PA-CP-E (1 kV) process was similar to that (89.0 ± 3.2%) of cell-embedding-hydrogel processed by PA-CP (Fig. 4(c)). However, cell viability decreased significantly as the applied voltage increased (2 and 3 kV), compared with the conventional process. Therefore, the PA-CP-E process using 1 kV did not reduce cell viability.

3.2. Strut-size distribution of the scaffolds

A homogenous strut size is a prerequisite for fabrication of an anatomically accurate, complex 3D cell-laden structure. Also, the pore structure (pore size, porosity, and interconnectivity) is an important design parameter, because the structure can directly affect various cellular activities—including viability, proliferation and differentiation—by mediating the transfer of nutrients and metabolic waste. The ability of the PA-CP and PA-CP-E processes to fabricate a one-layered mesh structure under constant
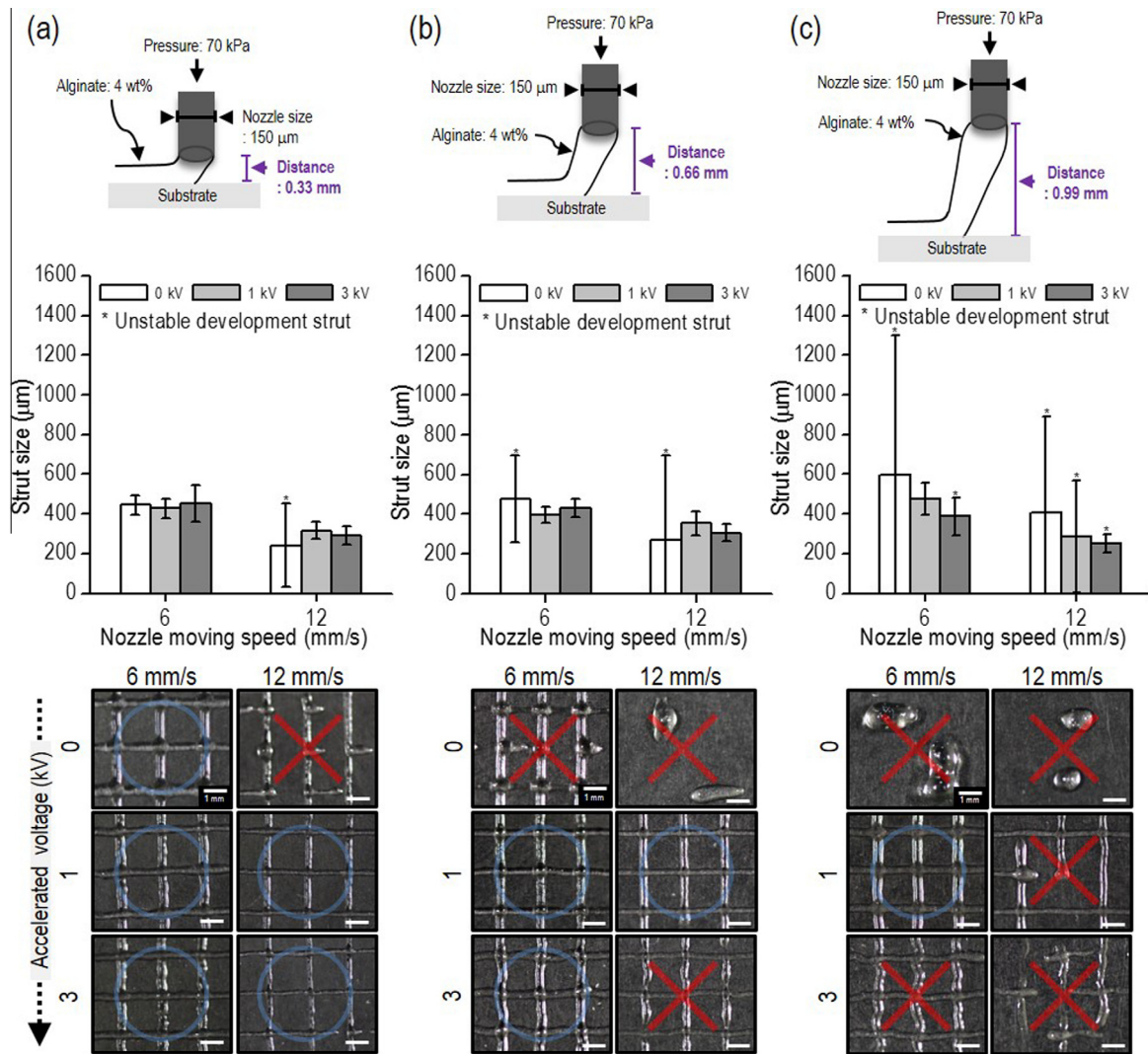
Fig. 5. Schematic diagram of the cell-printing process using distances of (a) 0.33 mm, (b) 0.66 mm, and (c) 0.99 mm between the nozzle tip and working stage, measured strut size, together with optical images of cell-laden mesh structures fabricated using various electric field strengths and nozzle movement speeds (n = 5). 'o' and 'x' indicate stable and unstable mesh structures, respectively. Asterisks (∗) indicate P < 0.05.

pneumatic pressure (70 ± 10 kPa), two nozzle movement speeds (6 and 12 mm s^{-1}), and three distances (0.33, 0.66, and 0.99 mm) between the nozzle tip and the working stage was evaluated (Fig. 5(a–c)). In the optical images, 'o' and 'x' indicate successful and unsuccessful printing of a mesh structure, respectively. Using the PA-CP process, mesh struts were not stably printed on the substrate, with the exception of that using a distance of 0.33 mm, due to clogging of the nozzle tip. However, application of an electric voltage (1 kV) significantly improved printability, with the exception of a distance of 0.99 mm. Also, when 3 kV was used in the PA-CP-E process, the printed mesh struts were slightly unstable due to the normal electric force ($\overrightarrow{F}_{ne}$). Therefore, the most homogenous mesh struts were obtained using the PA-CP-E process with an electric strength of 1 kV.

3.3. Optimal conditions for the PA-CP and PA-CP-E processes

To determine the optimum conditions for fabrication of cell-laden structures using the PA-CP and PA-CP-E (1, 3, and 5 kV) methods, four parameters (nozzle movement speed (NMS), distance between the nozzle tip and the working stage (D), measured electric current (C), and printed strut size (S)) were varied.

Fig. 6(a–d) shows optical images of cell-laden mesh structures fabricated using a nozzle movement speed of 12 mm s^{-1} and a distance of 0.33 mm. The mesh structure fabricated using PA-CP-E (1 kV) exhibited a well-designed mesh structure. To determine the optimum processing conditions, the quantitative values of the parameters (NMS, D, 1/C, 1/S, and C-V) shown in Fig. 6 were used. To achieve the optimal rate of 3D structure fabrication, the NMS and D values should be high; the 1/C, 1/S, and C-V values should be high to optimize cell activities post-fabrication.

As shown in the radial graphs, the NMS and D values of the cell-laden structure fabricated using PA-CP-E (1 kV) were higher than those of the structure fabricated using the conventional method. On the other hand, the structure fabricated using PA-CP-E (3 kV) process had significantly lower cell viability and higher electric current than those fabricated using the PA-CP and PA-CP-E (1 kV) processes. In addition, when 5 kV was used, the mesh structure was not stably fabricated due to generation of an electric spark between the nozzle and the substrate. Therefore, the PA-CP-E (1 kV) process resulted in fabrication of a structure that yielded optimal cell activity.
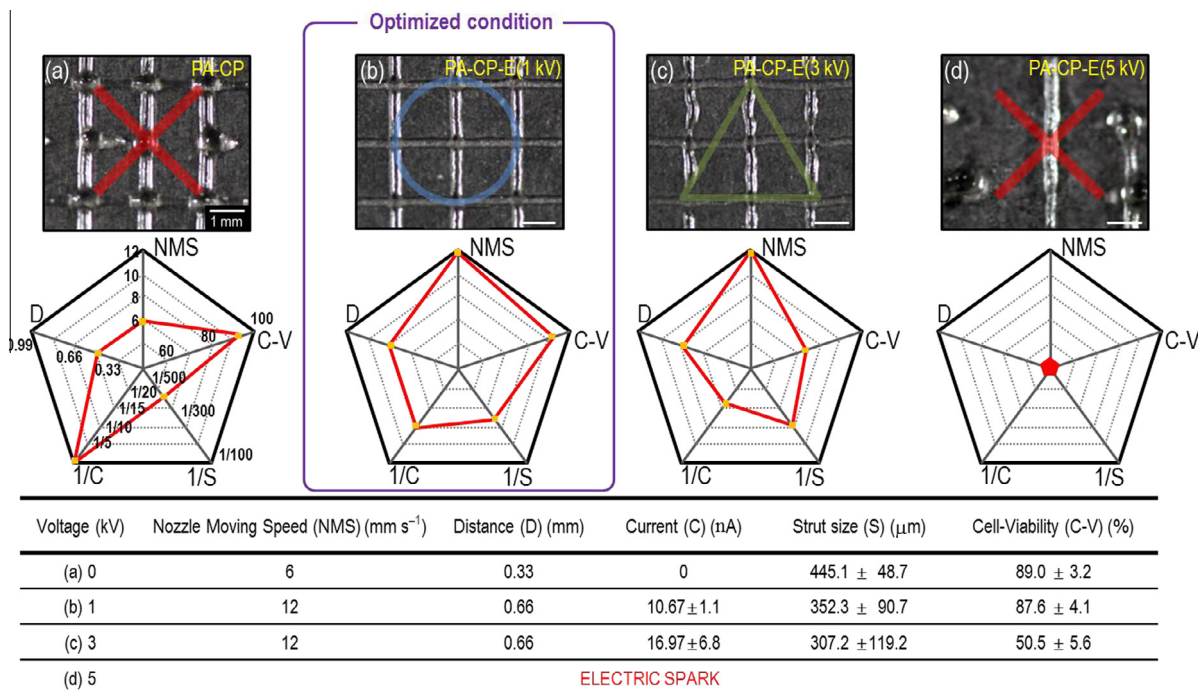
Fig. 6. Optical images ('x': unstable, 'o': stable, and 'Δ': intermediate structure) of structures fabricated using the (a) PA-CP process and the PA-CP-E with (b) 1 kV, (c) 3 kV, and (c) 5 kV processes. Radial graphs show the processing quality in terms of five processing parameters (nozzle movement speed (NMS), printable distance (D) between the nozzle tip and the working stage, measured electric current (C), printed strut size (S, n = 10), and cell viability (C-V, n = 5)). The values of the properties are shown in the table.

3.4. Cell viability according to volume flow rate and applied voltage

The PA-CP-E (1 kV) process was found to be optimal for cell printing. The relationships of volume flow rate and cell viability as a function of the applied pneumatic pressure during fabrication of extruded cell-laden struts by the PA-CP and PA-CP-E (1 kV) processes are described in Fig. 7. Fig. 7(a) shows a schematic diagram of the test. Fig. 7(b) shows that the PA-CP-E process induced a higher volume flow rate compared with the PA-CP process at the same pneumatic pressure, due to the electrostatic force directed to the working stage. In general, a higher volume flow rate results in higher wall shear stress, which reduces the viability of the cells within the cell-embedding-hydrogel [39]. However, although a high volume flow rate was obtained in the PA-CP-E process, a reduction in cell viability was not observed. Furthermore, the cell viability appeared to be independent of the applied pressure (Fig. 7(c)). This may have been due to the applied electrostatic force in the PA-CP-E process, which can pull the extruded strut of the cell-embedding-hydrogel at the nozzle tip to the dispensing stage, reducing the wall shear stress in the nozzle.

To observe the effect of the PA-CP-E (1 kV) with a nozzle with smaller diameter, we tested the printability and cell-viability of the cell-laden structures, which were fabricated using the PA-CP and PA-CP-E (1 kV). In the test, as shown in the image (Fig. 7(d)), the diameter of the nozzle was 150 μm and applied pneumatic pressure was 300 ± 27 kPa. As expected, the volume flow rate (4.1×10^{-3} cm^3 s^{-1}) of the cell-embedding-hydrogel using the PA-CP-E (1 kV) was much higher than that (3.0×10^{-3} cm^3 s^{-1}) of the PA-CP (Fig. 7(e)). In order to fabricate similar strut size (347 ± 46 μm for PA-CP and 332 ± 56 μm for PA-CP-E (1 kV)), we used different nozzle moving speed because the volume flow rate of the each process was different under the constant pressure. Fig. 7(f) show optical and fluorescent images of the cell-laden mesh structures, where live cells are green and dead cells are red. As shown in the images, the cells in both structures were well distributed throughout the mesh structure, but the cell-viability was

much higher in the cell-laden structure fabricated using the PA-CP-E (1 kV) compared to that of the structure using the PA-CP (Fig. 7(g)).

In the cell-printing process, the controllability of the printed strut diameter can be an important design parameter since the printed strut diameter can affect the cell-release and cell-growth of the cell-laden structure. Therefore, the diameter of the printed cell-embedding-hydrogel for various moving speeds of the nozzle (150 μm) using the PA-CP-E (1 kV) was measured in Fig. 7(h). The diameter of printed cell-laden struts increased linearly with decreasing nozzle moving speed without any sacrifice of cell-viability. To show the feasibility of the fabrication of 3D multi-layered structure using the PA-CP-E (1 kV), four-layered mesh structure (thickness = 1.1 mm) was fabricated with the nozzle (150 μm) and moving speed, 11.3 mm s^{-1}, (Fig. 7(i)).

Based on the results, we can confirm that the PA-CP-E (1 kV) can provide much safer processing condition of the cell-embedding-hydrogel and even have much more controllable processing window compared to the pure pressure-based cell printing process, PA-CP.

3.5. In vitro cell culture

Fig. 8(a–c) shows optical and SEM images of four-layered cell-laden structures fabricated using the PA-CP and PA-CP-Es (1 and 2 kV) processes to measure cell metabolic activities. The SEM images showed that the pore structure was maintained. Fig. 8(d) shows the result of MTT assay of cell proliferation in the cell-laden structures. At day 1, the number of viable cells was significantly higher in the structures fabricated using the PA-CP and PA-CP-E (1 kV) processes than in that fabricated using the PA-CP-E (2 kV) process. This is likely related to the initial cell viability after fabrication (Fig. 4(c)). The number of viable cells in all structures increased over time; however, the degree of proliferation was significantly lower in the structure fabricated using the PA-CP-E
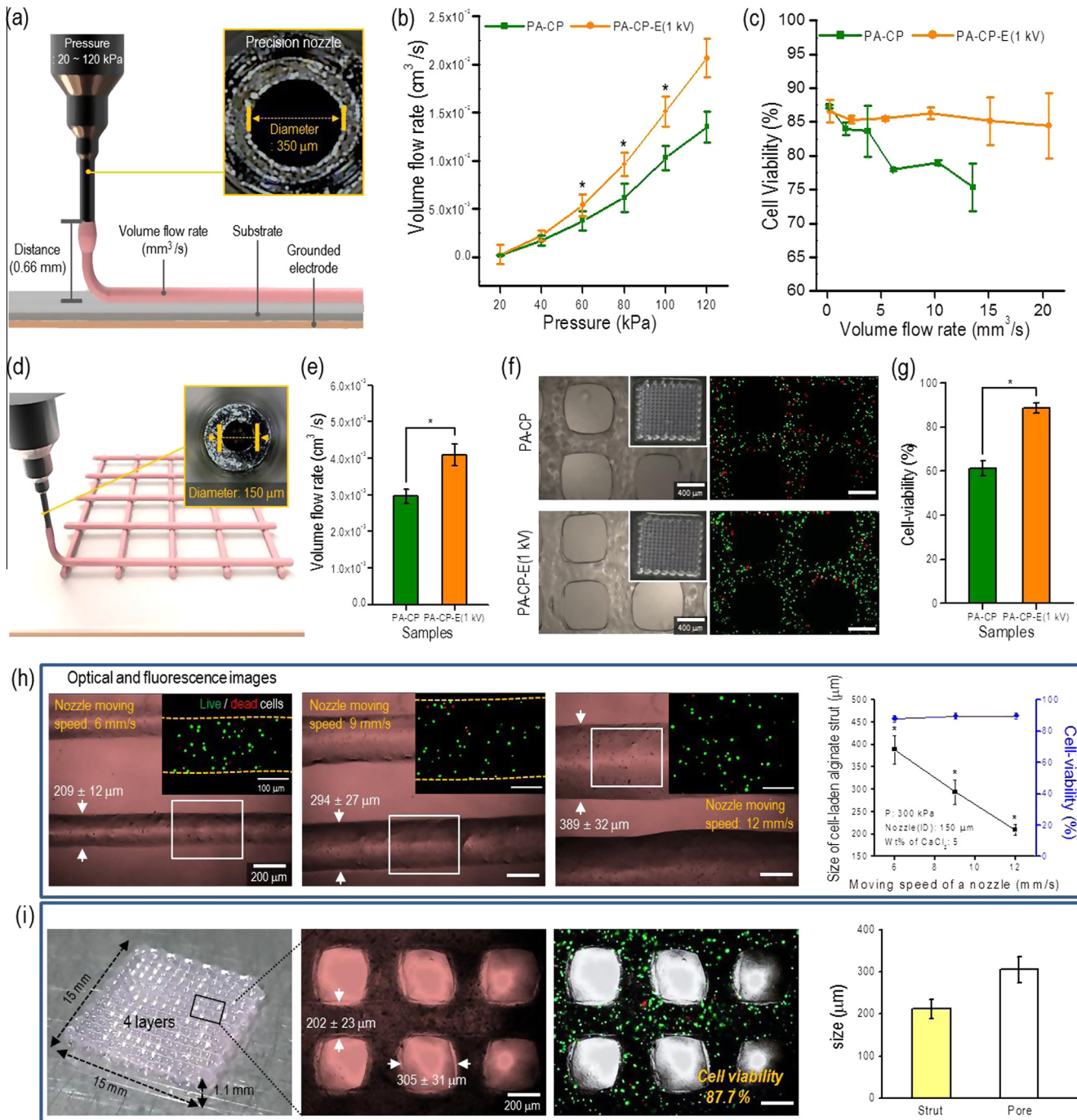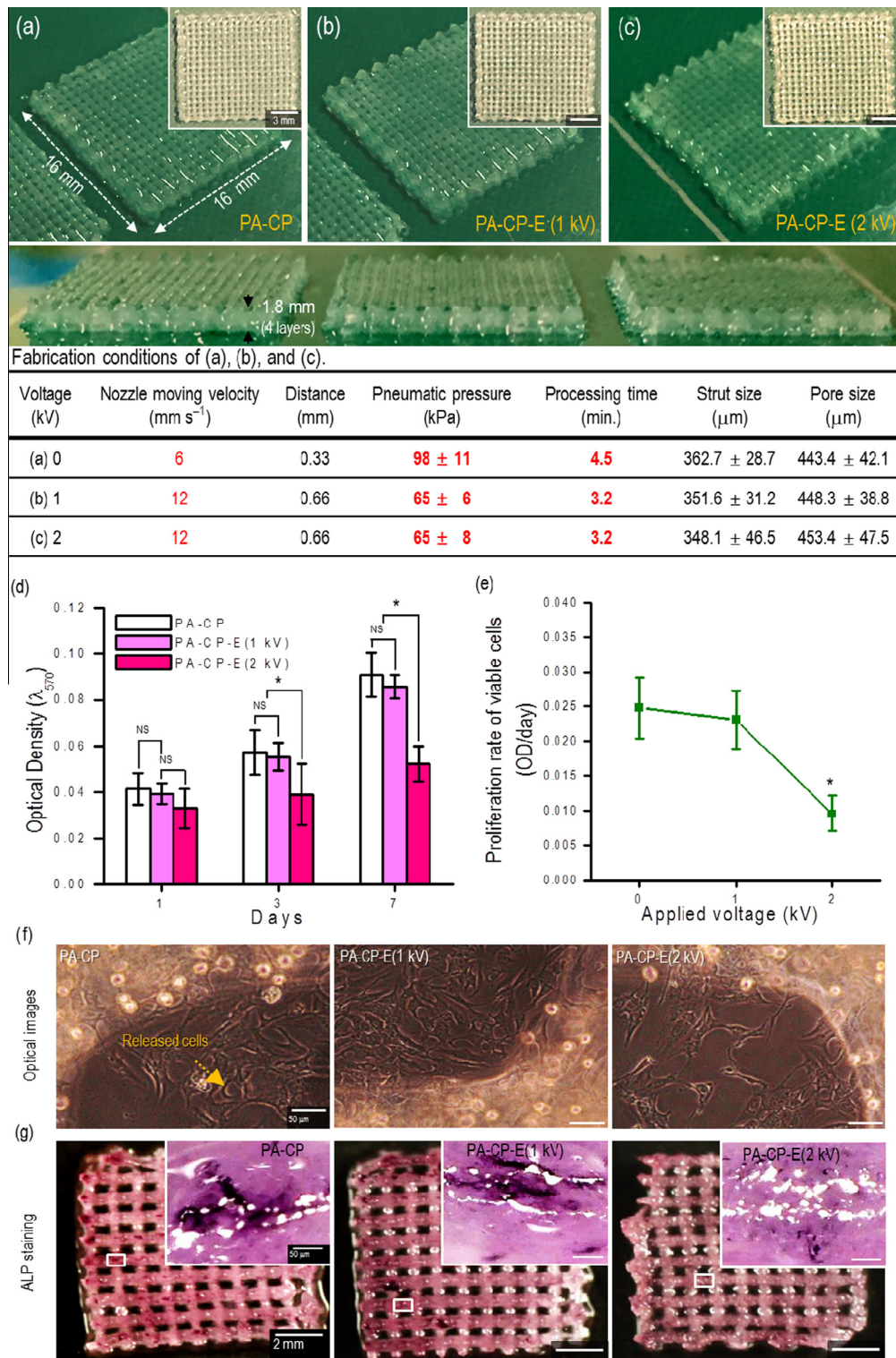
Fig. 7. (a) Schematic diagram of the parameters of the cell-printing process. (b) Volume flow rate as a function of pneumatic pressure (20–120 kPa) for the PA-CP and PA-CP-E (1 kV) processes (n = 5). (c) Cell viability as a function of the volume flow rate for the PA-CP and PA-CP-E (1 kV) processes (n = 5). (d) Schematic diagram of the fabrication process using a nozzle (150 μm) and (e) volume flow rate a constant pneumatic pressure (300 ± 27 kPa) for the PA-CP and PA-CP-E (1 kV) processes. (f) Optical and fluorescence images of the mesh structures and (g) cell-viability. (h) Size control of the printed struts at various moving speeds of a nozzle (150 μm) using PA-CP-E (1 kV) (n = 5). (i) Three-dimensional shape and fluorescence image of the printed mesh structure (15 × 15 × 1.1 mm³) (n = 5). Asterisks (∗) indicate $P < 0.05$.

(2 kV) process compared with the other structures. The difference in the proliferation rate (slope of optical density vs. time) of the cell-laden structures fabricated using the PA-CP and PA-CP-E (1 kV) processes was ∼6.8%, which was not significant (Fig. 8(e)). However, the difference between the cell-laden structures fabricated using the PA-CP-E (1 kV) and PA-CP-E (2 kV) processes was 58.4%, which was significant. Thus, the metabolic activities of cells within the structures fabricated using the PA-CP and PA-CP-E (1 kV) processes were similar. Fig. 8(f) shows optical images of cell

release after 7 days of culture from cell-laden structures fabricated using the PA-CP and PA-CP-E (1 kV and 2 kV) processes. Release of cells was greater from structures fabricated using the PA-CP and PA-CP-E (1 kV) processes.

The optical images of ALP activity of the cell-laden mesh structure (four-layers) cultured for 10 days were attained to qualitatively observe the differentiation (Fig. 8(g)). The ALP activity of the structure obtained using PA-CP was similar with that of the structure fabricated using PA-CP-E (1 kV), while the stained

Fabrication conditions of (a), (b), and (c).

Voltage (kV)	Nozzle moving velocity (mm s⁻¹)	Distance (mm)	Pneumatic pressure (kPa)	Processing time (min.)	Strut size (μm)	Pore size (μm)
(a) 0	6	0.33	98 ± 11	4.5	362.7 ± 28.7	443.4 ± 42.1
(b) 1	12	0.66	65 ± 6	3.2	351.6 ± 31.2	448.3 ± 38.8
(c) 2	12	0.66	65 ± 8	3.2	348.1 ± 46.5	453.4 ± 47.5

Fig. 8. Optical images and fabricating conditions of cell-laden structures fabricated using the (a) PA-CP and (b, c) PA-CP-E (1 and 2 kV) processes with the nozzle size (350 μm). (d) 3-(4,5-Dimethylthiazol-2-yl)-2,5-diphenyltetrazolium bromide (MTT) assay of cell proliferation after culture for 1, 3, and 7 days (n = 5). (e) Cell proliferation rate as a function of the applied voltage. (f) Release of cells from the cell-laden structures. (g) Optical images of alkaline phosphatase (ALP) activity. Asterisks (∗) indicate $P < 0.05$.

densities of the structures fabricated using PA-CP and PA-CP-E (1 kV) were meaningfully denser compared to that of the PA-CP-E (2 kV). The results mean that the structures fabricated using the PA-CP and PA-CP-E (1 kV) provided a similar microcellular environment for cell proliferation and osteogenic activity.

3.6. Fabrication of a hASC-laden pore structure using the PA-CP-E (1 kV) process

hASCs are used for cell therapy and tissue engineering because they can differentiate into a variety of cell types [45]. According to
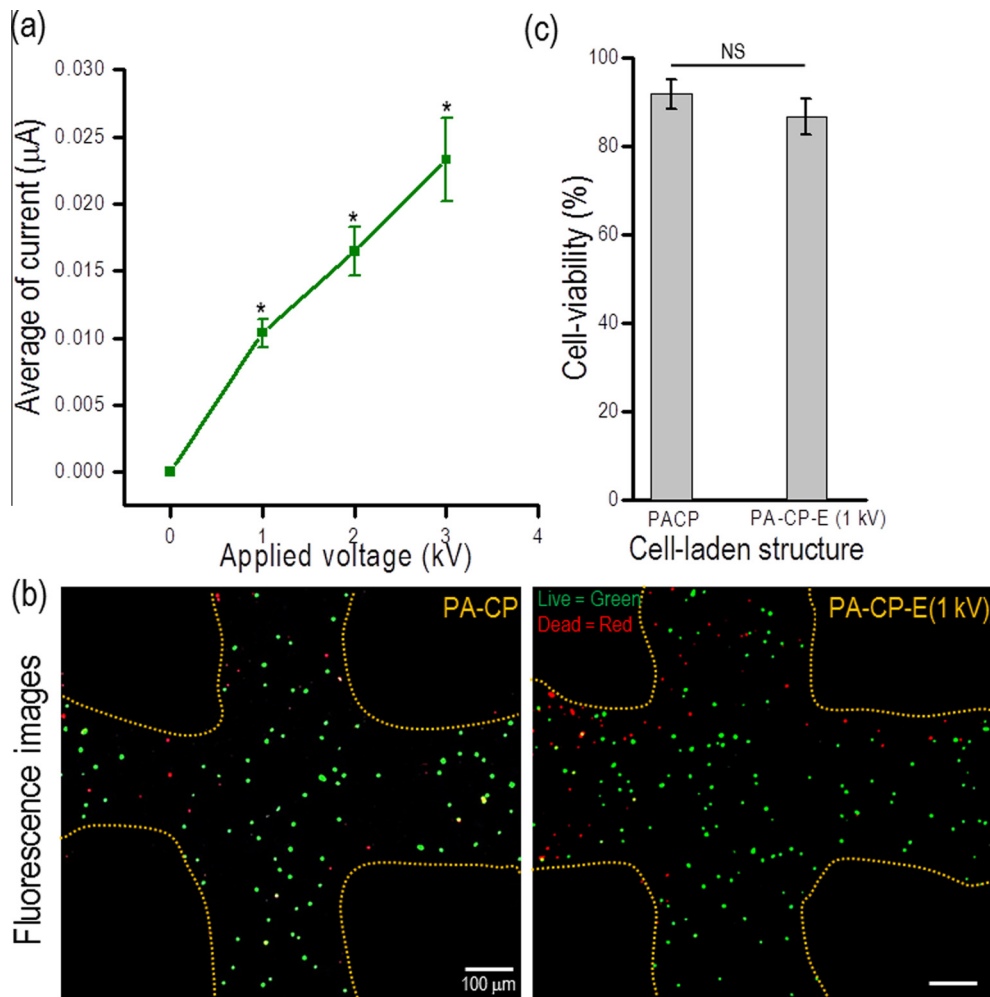
Fig. 9. (a) Relationship between applied voltage and measured current for the hydrogel with hASCs (n = 5). (b) Live (green)/dead (red)-stained images of hASCs-laden structures fabricated using the processes, PA-CP and PA-CP-E of 1 kV. (c) Plot of cell viability (as determined by live/dead staining) for the cell-laden structures (n = 5). Asterisks (∗) indicate *P* < 0.05 and 'NS' means non-significance. (For interpretation of the references to colour in this figure legend, the reader is referred to the web version of this article.)

Mizuno, hASCs exhibit the capacity to differentiate into various cells and tissues of mesodermal origin, similar to human bone marrow-derived mesenchymal stem cells [46]. Therefore, fabrication of highly porous and size-controllable hASCs-laden structures is an important part of tissue regeneration research and requires appropriate scaffolds, cells, and growth factors. To demonstrate the feasibility of the PA-CP-E (1 kV) process, multi-layered porous mesh structures laden with hASCs (1×10^6 mL^{-1}) were fabricated using conditions identical to those used for the MG63-laden structures shown in Fig. 8(b). Fig. 9(a) shows relationship between applied voltage and measured current for the hydrogel with hASCs and the relation was very similar with the cell-embedding-hydrogel consisting of the alginate and MG63. Fig. 9(b) shows a fluorescence image of live/dead cells for the dispensed structures using the PA-CP and PA-CP-E (1 kV). As shown in the Fig. 9(c), the viability of the hASCs in the structures fabricated using PA-CP and PA-CP-E (1 kV) exhibited 91.7 ± 3% and 86.6 ± 4%, respectively; it is statistically non-significant (*P* > 0.05). Therefore, the PA-CP-E (1 kV) process is suitable for fabrication of hASC-laden structures. However, as this work focused only on fabrication of porous 3D structures and the viability of hASCs, further studies that evaluate differentiation into various cell lineages both *in vitro* and *in vivo* are warranted.

4. Conclusion

We report here a hybrid direct-write cell printing strategy for fabricating cell-laden porous structures using pressure-assisted cell dispensing together with an electric field. The PA-CP-E (1 kV) process can provide much stable cell printed struts of the cell-embedding-hydrogel and significantly higher cell viability under a constant pneumatic pressure compared to the PA-CP. This was achieved by an electrostatic force generated using an electric field of an appropriate strength (1 kV). Furthermore, the cells in the 3D structure fabricated using the electric-field-assisted cell-printing process exhibited similar metabolic function during culture compared to those in a structure fabricated using a process without an electric field. Therefore, the modified cell-printing process facilitates efficient and rapid fabrication of porous 3D cell-laden structures that maintain the viability and proliferation of cells embedded therein, indicating that the technique has potential for tissue regeneration.

However, in this work the fabrication of high-thickness cell-laden structure (over four-layers) can be limited because of the interference of the remnant electrostatic charges of the cell-laden struts printed on the previous layer, but we expect that the usage of various hybrid architectures consisting of the cell-laden struts

and synthetic polymers will enable the fabrication of more thickened 3D cell-laden porous structures.

Acknowledgements

References

[1] J.J. Marler, J. Upton, R. Langer, J.P. Vacanti, Transplantation of cells in matrices for tissue regeneration, Adv. Drug Deliv. Rev. 33 (1998) 165–182.

[2] Q.P. Pham, U. Sharma, A.G. Mikos, Electrospinning of polymeric nanofibers for tissue engineering applications: a review, Tissue Eng. 12 (2006) 1197–1211.

[3] I. Stanasel, M. Mirzazadeh, J.J. Smith, Bladder tissue engineering, Urol. Clin. North Am. 37 (2010) 593–599.

[4] M. Boffito, S. Sartori, G. Ciardelli, Polymeric scaffolds for cardiac tissue engineering: requirements and fabrication technologies, Polym. Int. 63 (2014) 2–11.

[5] F. Groeber, M. Holeiter, M. Hampel, S. Hinderer, K. Schenke-Layland, Skin tissue engineering—in vivo and in vitro applications, Adv. Drug Deliv. Rev. 63 (2011) 352–366.

[6] B.O. Diekman, N. Christoforou, V.P. Willard, H. Sun, J. Sanchez-Adams, K.W. Leong, et al., Cartilage tissue engineering using differentiated and purified induced pluripotent stem cells, PNAS 109 (2012) 19172–19177.

[7] I.L. Kim, R.L. Mauck, J.A. Burdick, Hydrogel design for cartilage tissue engineering: a case study with hyaluronic acid, Biomaterials 32 (2011) 8771–8782.

[8] S. Bose, M. Roy, A. Bandyopadhyay, Recent advances in bone tissue engineering scaffolds, Trends Biotechnol. 30 (2012) 546–554.

[9] B. Chan, K. Leong, Scaffolding in tissue engineering: general approaches and tissue-specific considerations, Eur. Spine J. 17 (2008) 467–479.

[10] Y. Du, E. Lo, S. Ali, A. Khademhosseini, Directed assembly of cell-laden microgels for fabrication of 3D tissue constructs, PNAS 105 (2008) 9522–9527.

[11] N.E. Fedorovich, J. Alblas, W.E. Hennink, F.C. Öner, W.J. Dhert, Organ printing: the future of bone regeneration?, Trends Biotechnol 29 (2011) 601–606.

[12] N.E. Fedorovich, W. Schuurman, H.M. Wijnberg, H.-J. Prins, P.R. van Weeren, J. Malda, J. Alblas, W.J. Dhert, Biofabrication of osteochondral tissue equivalents by printing topologically defined, cell-laden hydrogel scaffolds, Tissue Eng. Part C 18 (2011) 33–44.

[13] B. Guillotin, F. Guillemot, Cell patterning technologies for organotypic tissue fabrication, Trends Biotechnol. 29 (2011) 183–190.

[14] V. Mironov, R.P. Visconti, V. Kasyanov, G. Forgacs, C.J. Drake, R.R. Markwald, Organ printing: tissue spheroids as building blocks, Biomaterials 30 (2009) 2164–2174.

[15] C.M. Smith, A.L. Stone, R.L. Parkhill, R.L. Stewart, M.W. Simpkins, A.M. Kachurin, W.L. Warren, S.K. Williams, Three-dimensional bioassembly tool for generating viable tissue-engineered constructs, Tissue Eng. 10 (2004) 1566–1576.

[16] D. Chrisey, A. Pique, R. Modi, H. Wu, R. Auyeung, H. Young, Direct writing of conformal mesoscopic electronic devices by MAPLE DW, Appl. Surf. Sci. 168 (2000) 345–352.

[17] U. Demirci, G. Montesano, Cell encapsulating droplet vitrification, Lab Chip 7 (2007) 1428–1433.

[18] R.J. Klebe, Cytoscribing: a method for micropositioning cells and the construction of two-and three-dimensional synthetic tissues, Exp. Cell Res. 179 (1988) 362–373.

[19] D.B. Kolesky, R.L. Truby, A. Gladman, T.A. Busbee, K.A. Homan, J.A. Lewis, 3D bioprinting of vascularized, heterogeneous cell-laden tissue constructs, Adv. Mater. 26 (2014) 3124–3130.

[20] L. Koch, A. Deiwick, B. Chichkov, Laser-based 3D cell printing for tissue engineering, BioNanoMaterials 15 (2014) 71–78.

[21] F. Xu, T.D. Finley, M. Turkaydin, Y. Sung, U.A. Gurkan, A.S. Yavuz, R.O. Guldiken, U. Demirci, The assembly of cell-encapsulating microscale hydrogels using acoustic waves, Biomaterials 32 (2011) 7847–7855.

[22] J. Fuh, Micro-and Bio-rapid prototyping using drop-on-demand 3D printing, in: Handbook of Manufacturing Engineering and Technology, Springer, 2014, pp. 1–15.

[23] S. Ahn, H. Lee, L.J. Bonassar, G. Kim, Cells (MC3T3-E1)-laden alginate scaffolds fabricated by a modified solid-freeform fabrication process supplemented with an aerosol spraying, Biomacromolecules 13 (2012) 2997–3003.

[24] S. Ahn, H. Lee, E.J. Lee, G. Kim, A direct cell printing supplemented with low-temperature processing method for obtaining highly porous three-dimensional cell-laden scaffolds, J. Mater. Chem. B 2 (2014) 2773–2782.

[25] S.H. Ahn, H.J. Lee, J.-S. Lee, H. Yoon, W. Chun, G.H. Kim, A novel cell-printing method and its application to hepatogenic differentiation of human adipose stem cell-embedded mesh structures, Sci. Rep. 5 (2015) 13427.

[26] B.R. Ringeisen, C.M. Othon, J.A. Barron, D. Young, B.J. Spargo, Jet-based methods to print living cells, Macromol. Biosci. 1 (2006) 930–948.

[27] E.A. Roth, T. Xu, M. Das, C. Gregory, J.J. Hickman, T. Boland, Inkjet printing for high-throughput cell patterning, Biomaterials 25 (2004) 3707–3715.

[28] F. Guillemot, A. Souquet, S. Catros, B. Guillotin, Laser-assisted cell printing: principle, physical parameters versus cell fate and perspectives in tissue engineering, Nanomedicine 5 (2010) 507–515.

[29] X. Cui, D. Dean, Z.M. Ruggeri, T. Boland, Cell damage evaluation of thermal inkjet printed Chinese hamster ovary cells, Biotechnol. Bioeng. 106 (2010) 963–969.

[30] B. Derby, Bioprinting: inkjet printing proteins and hybrid cell-containing materials and structures, J. Mater. Chem. 18 (2008) 5717–5721.

[31] C. Born, Z. Zhang, M. Al-Rubeai, C. Thomas, Estimation of disruption of animal cells by laminar shear stress, Biotechnol. Bioeng. 40 (1992) 1004–1010.

[32] S.V. Murphy, A. Atala, 3D bioprinting of tissues and organs, Nat. Biotechnol. 32 (2014) 773–785.

[33] H. Kawamoto, S. Umezu, R. Koizumi, Fundamental investigation on electrostatic ink jet phenomena in pin-to-plate discharge system, J. Imaging Sci. Technol. 49 (2005) 19–27.

[34] L. Gasperini, D. Maniglio, A. Motta, C. Migliaresi, An electrohydrodynamic bioprinter for alginate hydrogels containing living cells, Tissue Eng. Part C 21 (2014) 123–132.

[35] M.J. Poellmann, K.L. Barton, S. Mishra, A.J.W. Johnson, Patterned hydrogel substrates for cell culture with electrohydrodynamic jet printing, Macromol. Biosci. 11 (2011) 1164–1168.

[36] P.A. Eagles, A.N. Qureshi, S.N. Jayasinghe, Electrohydrodynamic jetting of mouse neuronal cells, Biochem. J. 394 (2006) 375–378.

[37] C.S. Lee, J.P. Gleghorn, N.W. Choi, M. Cabodi, A.D. Stroock, L.J. Bonassar, Integration of layered chondrocyte-seeded alginate hydrogel scaffolds, Biomaterials 28 (2007) 2987–2993.

[38] S. Ahn, H. Lee, J. Puetzer, L.J. Bonassar, G. Kim, Fabrication of cell-laden three-dimensional alginate-scaffolds with an aerosol cross-linking process, J. Mater. Chem. 22 (2012) 18735–18740.

[39] R. Hartman, J.-P. Borra, D. Brunner, J. Marijnissen, B. Scarlett, The evolution of electrohydrodynamic sprays produced in the cone-jet mode, a physical model, J. Electrostat. 47 (1999) 143–170.

[40] R.P.A. Hartman, D. Brunner, D. Camelot, J. Marijnissen, B. Scarlett, Electrohydrodynamic atomization in the cone–jet mode physical modeling of the liquid cone and jet, J. Aerosol Sci. 30 (1999) 823–849.

[41] A. Khan, K. Rahman, D.S. Kim, K.H. Choi, Direct printing of copper conductive micro-tracks by multi-nozzle electrohydrodynamic inkjet printing process, J. Mater. Process. Technol. 212 (2012) 700–706.

[42] S.N. Jayasinghe, Cell electrospinning: a novel tool for functionalising fibres, scaffolds and membranes with living cells and other advanced materials for regenerative biology and medicine, Analyst 138 (2013) 2215–2223.

[43] M. Yeo, G. Kim, Fabrication of cell-laden electrospun hybrid scaffolds of alginate-based bioink and PCL microstructures for tissue regeneration, Chem. Eng. J. 275 (2015) 27–35.

[44] M. Li, X. Tian, N. Zhu, D.J. Schreyer, X. Chen, Modeling process-induced cell damage in the biodispensing process, Tissue Eng. Part C 16 (2010) 533–542.

[45] A. Kodali, T.C. Lim, D.T. Leong, Y.W. Tong, Cell-microsphere constructs formed with human adipose-derived stem cells and gelatin microspheres promotes stemness, differentiation, and controlled pro-angiogenic potential, Macromol. Biosci. 14 (2014) 1458–1468.

[46] H. Mizuno, Adipose-derived stem cells for tissue repair and regeneration: ten years of research and a literature review, J. Nippon Med. Sch. 76 (2009) 56–66.